SUPPLEMENTARY INFORMATION

High quality large area $MoSe_2$ and $MoSe_2/Bi_2Se_3$ heterostructures on AlN(0001)/Si(111) substrates by molecular beam epitaxy

E. Xenogiannopoulou,[a] P. Tsipas,[a] K. E. Aretouli,[a] D. Tsoutsou,[a] S. A. Giamini,[a] C. Bazioti,[b] G. P. Dimitrakopulos,[b] Ph. Komninou,[b] S. Brems,[c] C. Huyghebaert,[c] I. P. Radu,[c] and A. Dimoulas*[a]

[a] Institute of Nanoscience and Nanotechnology, NCSR DEMOKRITOS, GR-15310, Athens, Greece. *E-mail: dimoulas@ims.demokritos.gr.

[b] Physics Department, Aristotle University of Thessaloniki, GR-54124 Thessaloniki, Greece.

[c] Imec, Kapeldreef 75, Leuven, Belgium.

Crystal structure of $MoSe_2$

Fig. S1a shows the crystal structure of the $2H_b$ structure of $MoSe_2$ along with the structural parameters of the direct lattice[S1]. The ball and stick models in Fig. S1b-c depict the structure of 3 ML $MoSe_2$ grown on AlN(0001), along the $[11\text{-}20]_{AlN}$ and $[1\text{-}100]_{AlN}$ directions. It can be inferred that along the $[1\text{-}100]_{AlN}$ direction the atoms are densely spaced.

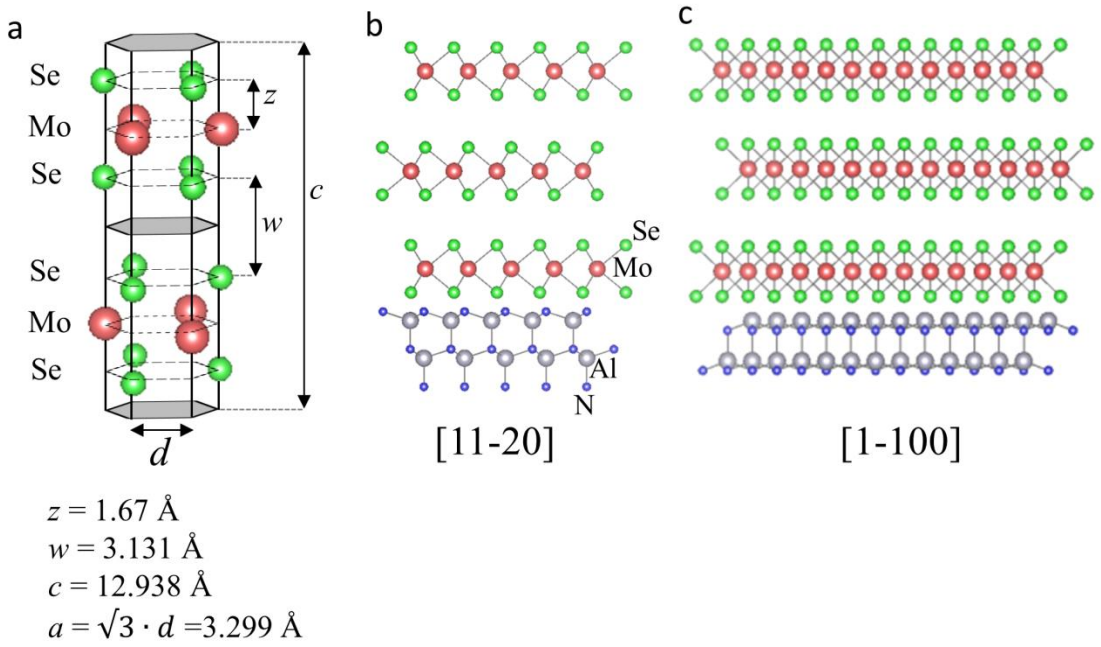

$z = 1.67$ Å
$w = 3.131$ Å
$c = 12.938$ Å
$a = \sqrt{3} \cdot d = 3.299$ Å

Fig. S1 (a) Crystal structure of 2H polytype of $MoSe_2$, (b-c). Stick and ball model of 3ML $MoSe_2$ structure deposited on AlN(0001), showing the $[11\text{-}20]_{AlN}$ (b) and $[1\text{-}100]_{AlN}$ (c) axis orientation, respectively.

Large area STM images of 3 ML $MoSe_2$/AlN

To enlighten the effect of the two-steps process of $MoSe_2$/AlN film growth on the film roughness and quality, large area STM images were acquired after each step. A (5x5) μm^2 STM image is given in Fig. S2a showing that after the deposition at 350 °C, a continuous full covered $MoSe_2$ film is formed while after the post-deposition step at 690 °C (Fig. S2c) the film remains continuous, but the surface quality is improved becoming smoother and more homogeneous. The respective line profiles along the surface X-direction (blue lines) are also given in Figs. S2b and S2d, indicating that after the post-deposition annealing the surface becomes smoother. The root-mean-square (RMS) surface roughness values for the $MoSe_2$/AlN sample areas of (5x5) μm^2 was calculated 1.25 nm after the deposition step (Fig. S2a, b) and 0.62 nm after the post-deposition annealing step (Fig. S2c, d). For STM areas of (290x290) nm^2 the RMS values are 1.07 nm and 0.3nm for the 1st and 2nd process steps, respectively. The large area STM images and the calculated RMS values indicate that after the post-deposition annealing the $MoSe_2$/AlN film has a smooth morphology on average. A few higher-roughness areas (white areas~ 5nm height and yellow areas~2 nm height) are formed.

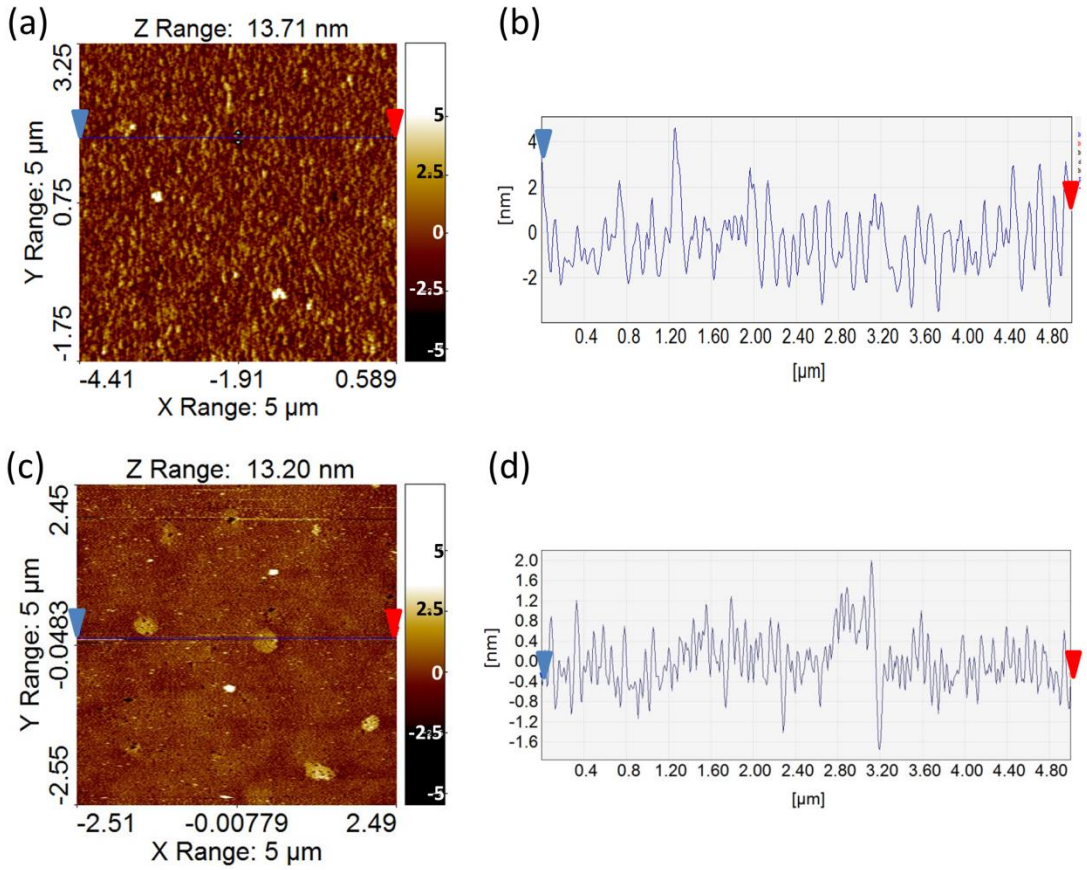

Fig. S2 (5x5) μm^2 STM images of the 3 ML $MoSe_2$/AlN surface (a) after the deposition at the relative low temperature of 350 °C and (c) after the post-deposition annealing at 690 °C (b, d) Equivalent line profiles along the surface X-direction (blue line in (a) and (c), respectively, showing that the surface roughness and the film uniformity are improved after the post-deposition annealing step.

Large area optical and SEM images of $MoSe_2$ films on AlN

Optical images of large area $MoSe_2$ films on AlN with variable thickness are shown in Fig. S3a, b. At the substrate edges the bare AlN is distinguished from $MoSe_2$ deposited films. This is due to a masking effect caused from mounting the sample to the sample holder. The optical images indicate that the various deposited $MoSe_2$ films are uniform and of high quality in the large range of 2´´ wafers. The high quality and uniformity can also be verified by the SEM images for 2ML and 3ML $MoSe_2$ films given in Figs. S3c and S3d, respectively. Fig. S3c is taken from the sample center indicating the film continuity, while Fig. S3d is from the sample edge, showing the bare AlN near the edge and the deposited film $MoSe_2$ film on top.

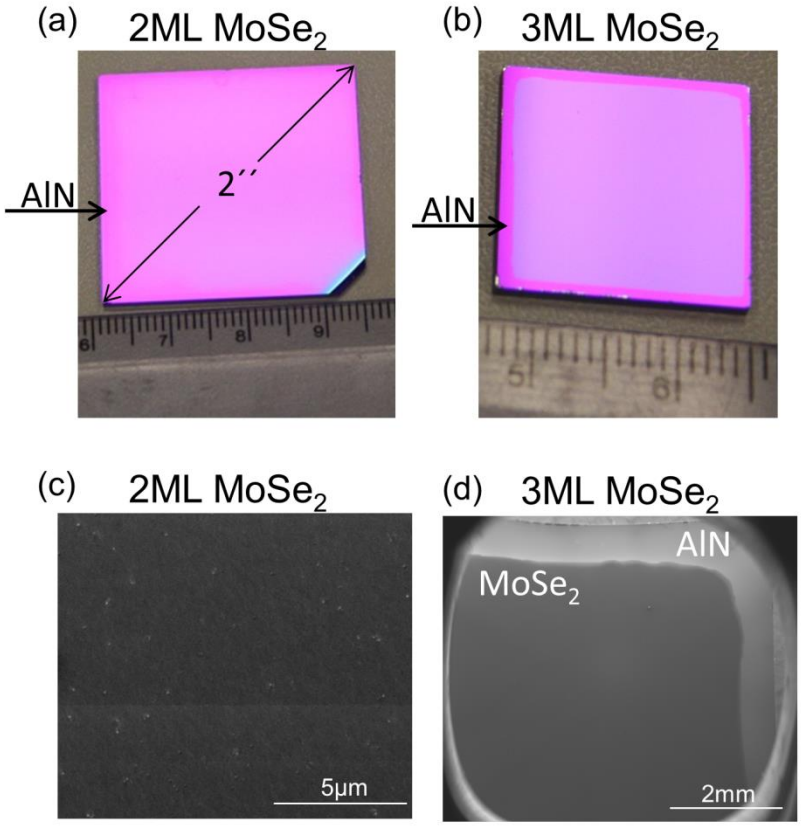

Fig. S3 (a, b) Photos of 2ML and 3ML $MoSe_2$ film deposited on AlN substrates. The substrate in (a) has 2´´diagonal, while in (b) the side dimension is 17.5mm. (c, d) SEM images of 2ML and 3ML $MoSe_2$ film on AlN showing a high quality, continuous film.

GPA lattice strain analysis map of 3ML $MoSe_2$ deposited on AlN

Fig. S4 shows an increase of the lattice parameter by up to ~20% prior to the $MoSe_2$ film. Hexagonal molybdenum nitride has a 13% larger lattice constant than AlN along the growth direction[S2] so we suspect that some elastic strain is also present. A more detailed structural analysis of this region is out of the scope of the present work.

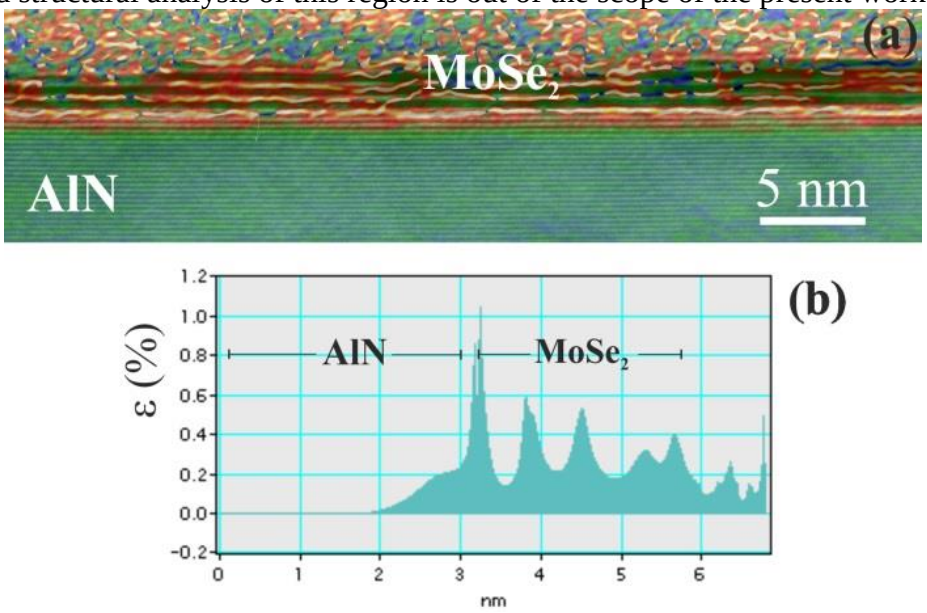

Fig. S4. (a) GPA lattice strain map obtained using the *g*0002 spatial frequency of AlN. The spatial resolution is 0.5 nm. The strain map is shown superimposed on the corresponding HRTEM image viewed along $[1\text{-}100]_{AlN}$. (b) Corresponding strain profile along the growth direction. A gradual increase of the strain up to ~20% is observed inside the AlN substrate.

Band diagrams reconstruction of $MoSe_2$/AlN and $MoSe_2/Bi_2Se_3$/AlN

The band structure of the $MoSe_2$/AlN heterojunction, depicted in Fig. 4e, was constructed according to Kraut's method by XPS measurements[S3]. Specifically the valence and conduction band offsets (VBO, CBO) for the $MoSe_2$/AlN heterojunction were calculated using the following equations:

$$VBO = \left(E_{Mo3d5/2} - VBM\right)_{MoSe2} - \left(E_{Al2p} - VBM\right)_{AlN} - (E_{Mo3d5/2} - E_{Al2p})_{AlN/MoSe2} \quad \text{(Eq. 1)}$$

$$CBO = \left(E_g\right)_{AlN} - \left(E_g\right)_{MoSe2} - VBO \quad \text{(Eq. 2)}$$

where $E_{Mo3d5/2}$ and E_{Al2p} are the core level energies, whereas VBM are the corresponding valence band maxima. The energy differences between the selected core levels and VBM are measured in bulk samples. Similar equations were applied for the determination of VBO and CBO for the $MoSe_2/Bi_2Se_3$/AlN heterojunction considering the two successive Bi_2Se_3/AlN and $MoSe_2/Bi_2Se_3$ structures (Fig. 4f). In this case, the core level energy of $Bi4f_{7/2}$ was employed for the XPS analysis. Finally, band gap energies (E_g) for AlN (6.2 eV), $MoSe_2$ (1.58 eV- from PL measurements reported in the main text and taking into account the reduction due to the exciton binding energy) and Bi_2Se_3 (0.47 eV[S4]) were applied for the CBO calculation.

The valence band offsets (VBO) have been derived to be 2.84 eV and 2.87 eV/0.1 eV for the $MoSe_2$ /AlN and $MoSe_2/Bi_2Se_3$/AlN samples, respectively. Accordingly, the conduction band offsets (CBO) have been calculated to be 1.81 eV

and 2.86 eV/0.98 eV for the $MoSe_2$/AlN and $MoSe_2/Bi_2Se_3$/AlN samples. The band diagrams of the $MoSe_2$/AlN and $MoSe_2/Bi_2Se_3$/AlN heterojunctions, shown in Fig. 4e, f of the main text, were reconstructed assuming reported electron affinities for the three materials (χ_{AlN}=2.1 eV[S5], χ_{MoSe2}=3.9 eV[S6], χ_{Bi2Se3}=5.06 eV[S7]).

Short scale uniformity investigation of 1ML $MoSe_2$ on AlN(0001)

Raman was performed on a square area (40 ×40) μm^2. The $MoSe_2$ A_{1g} Raman peak is analyzed and fitted with a Lorentz peak function and the results are resented in Fig. S5. It is found that there is very little variation in peak intensity (Fig. S5a), full width at half maximum (Fig. S5b), and position (Fig. S5c), which amount to about 11%, 3% and 0.1%, respectively. In addition, Fig. S5e shows the A_{1g}/E^1_{2g} Raman peak ratio mapping giving values very close to ~ 23. These results indicate that the $MoSe_2$ layer is very uniform.

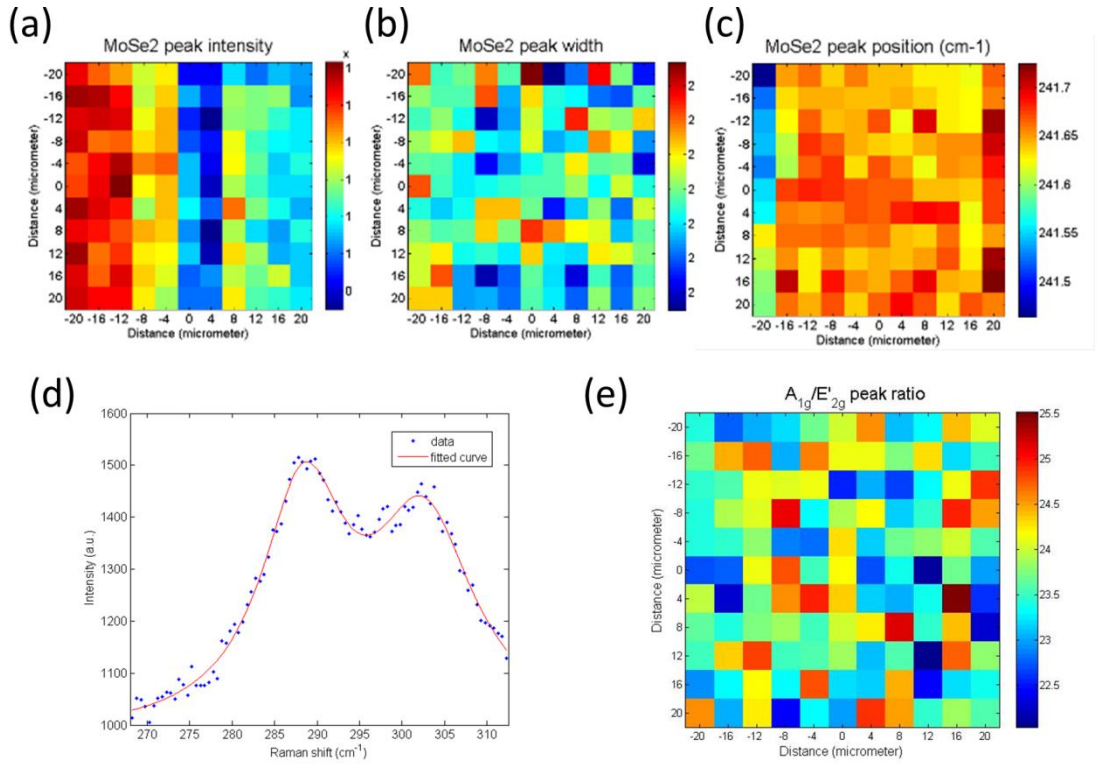

Fig. S5 (a-c) (40 ×40) μm^2 short scale mapping of the A_{1g} Raman peak intensity (a), half width at half maximum (b) and peak position (c). (d) Example of E^1_{2g} peak fitting and (e) the A_{1g}/E^1_{2g} Raman peak ratio map presents a value of ~ 23, indicating a uniform $MoSe_2$ layer.

Stability investigation of 1ML $MoSe_2$ on AlN(0001)

The layers are uncapped and after the growth are stored in vacuum bags until they are opened for the first time for Raman measurements (Fig. S6, left). Then, they are left

in air and measured again after 7 days (Fig. S6, middle) and then after 15 days (Fig. S6, right). No significant degradation of the Raman signal is observed indicating very good stability in air.

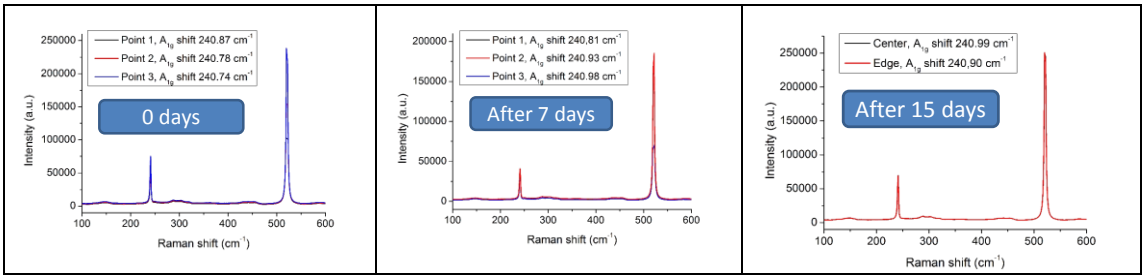

Fig. S6 Raman characterization on uncapped 1 ML $MoSe_2$ showing no or little degradation over a period of 15 days.

Large area TEM image of $MoSe_2$ on AlN(0001)

The larger area TEM image (Fig. S7) shows that the $MoSe_2$ film continuity and uniformity can be appreciated over a region that exceeds 250 nm in length.

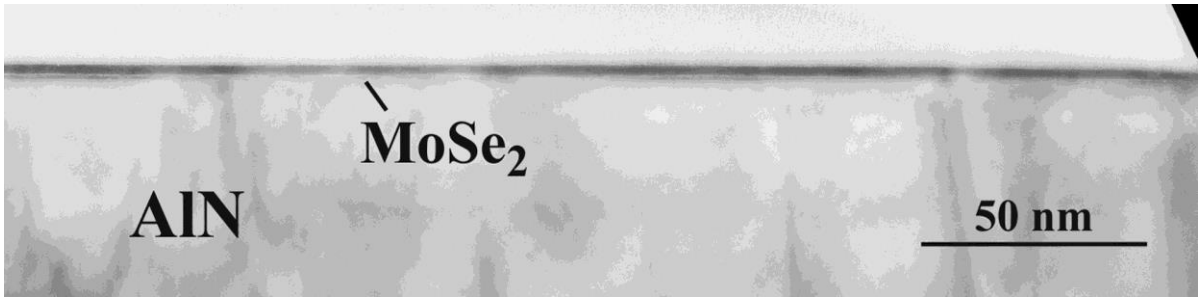

Fig. S7 Low magnification cross sectional bright field TEM showing $MoSe_2$ film continuity.

References

S1 R. Coehoorn, C. Haas, J. Dijkstra, C. J. F. Flipse, R. A. de Groot and A. Wold, *Phys. Rev. B*, 1987, **35**, 6195-6202.

S2 A. Bezinge, K. Yvon, J. Muller, W. Lengaeur and P. Ettmayer, *Solid State Commun.*, 1987, **63**, 141.

S3 E. Kraut, R. Grant, J. Waldrop and S. Kowalczyk, *Phys. Rev. Lett.*, 1980, **44**, 1620.

S4 P. Tsipas, E. Xenogiannopoulou, S. Kassavetis, D. Tsoutsou, E. Golias, C. Bazioti, G. P. Dimitrakopulos, P. Komninou, H. Liang, M. Caymax and A. Dimoulas, *ACS Nano*, 2014, **8**, 6614-6619.

S5 C. I. Wu, A, Kahn, E. S. Hellman and D. N. E. Buchanan, *Appl. Phys. Lett.*, 1998, **73**, 1346-1348.

S6 C. Gong, H. Zhang, W. Wang, L. Colombo, R. M. Wallace and K. Cho, *Appl. Phys. Lett.*, 2013, **103**, 053513.

S7 J. Suh, D. Fu, X. Liu, J. K. Furdyna, K. M. Yu, W. Walukiewicz, and J. Wu, *Phys. Rev. B*, 2014, **89**, 115307.